

Adaptive Learning on the Grids for Elliptic Hemivariational Inequalities

Jianguo Huang (jghuang@sjtu.edu.cn)

School of Mathematical Sciences, and MOE-LSC,
Shanghai Jiao Tong University, Shanghai 200240, China

Chunmei Wang (chunmei.wang@ttu.edu)

Department of Mathematics & Statistics,
Texas Tech University, 1108 Memorial Circle, Lubbock, TX 79409, USA

Haoqin Wang (wanghaoqin@sjtu.edu.cn)

School of Mathematical Sciences, and MOE-LSC,
Shanghai Jiao Tong University, Shanghai 200240, China

Abstract

This paper introduces a deep learning method for solving an elliptic hemivariational inequality (HVI). In this method, an expectation minimization problem is first formulated based on the variational principle of underlying HVI, which is solved by stochastic optimization algorithms using three different training strategies for updating network parameters. The method is applied to solve two practical problems in contact mechanics, one of which is a frictional bilateral contact problem and the other of which is a frictionless normal compliance contact problem. Numerical results show that the deep learning method is efficient in solving HVIs and the adaptive mesh-free multigrid algorithm can provide the most accurate solution among the three learning methods.

Keywords. Deep Learning; Elliptic Hemivariational Inequalities; Contact Problems; Mesh-Free Methods; Multigrid.

1 Introduction

This paper considers an efficient numerical method for solving an elliptic hemivariational inequality (HVI), which was first introduced by Panagiotopoulos in the context of engineering in the early 1980s [50]. After Panagiotopoulos' pioneering work, a lot of mathematical effort has been devoted to the study of HVIs (e.g., [51, 49, 48, 44, 22]), and HVIs have become a powerful mathematical tool in contact mechanics. In practice, the solution to elliptic HVIs is only available numerically. There have been various numerical methods to approximate the solution of elliptic HVIs (e.g., see [26, 23, 24, 19, 59]). After discretization, we often need to solve a non-convex and non-smooth optimization problem, which is challenging and technical to attack. One of the most popular methods for this non-convex optimization is the iterative convexification approach [58, 45], where a sequence of convex problems approaching the original non-convex problem is constructed and solved. Based on this iterative convexification approach, many HVIs describing contact problems

were solved, such as the frictional bilateral contact problem [3, 25], the frictionless normal compliance contact problem [4, 25], and the frictionless unilateral contact problem [25]. Except for the iterative convexification approach, other alternative choices are the proximal bundle method (e.g., see [42]), the bundle Newton method (e.g., see [2]), and the primal-dual active-set algorithm [36]. Recently, Feng, Han and Huang [19] used the double bundle method (cf. [33]) to solve the discrete non-convex and non-smooth problem arising from discretization of some HVIs. As a whole, the existing numerical approaches mentioned above are rather involved to implement in practice.

With the advance of deep learning techniques originated in computer science, considerable attention in applied mathematics and computational mathematics has been drawn to apply deep learning to scientific computing, especially for numerical methods to solve the partial differential equations (PDEs). Neural network-based numerical methods for solving PDEs date back to the 1990s [39, 13, 38] and achieve significant improvement recently (e.g., see [43, 54, 53, 57, 21, 34]). In those methods, deep neural networks (DNNs) are applied to parametrize PDE solutions and appropriate parameters are identified by minimizing an optimization problem formulated from the given PDE. The key to the success of neural networks-based methods is the universal approximation property of DNNs (cf. [29, 12, 28, 5, 37, 61, 62, 16, 55, 46, 47, 41, 17, 56]). Though deep learning has made great achievements in solving PDEs, especially in high-dimensional cases [21], it is also challenging to obtain a highly accurate solution. Recently, several deep learning frameworks have been developed along this line. For instance, E and Yu proposed the Deep Ritz method for high-dimensional variational problems [18]. Karniadakis and his team designed several neural networks by incorporating physical information [52, 32, 31]. Gu, Yang and Zhou developed the SelectNet to adaptively choose training samples in the learning process [20]. Liang et al. discussed how to design data-driven activation functions in [40]. Bao and his team introduced weak adversarial networks to find the weak solution of PDEs in [63]. Chen et al. proposed Friedrichs learning strategies to solve various PDEs in a unified way [9]. Huang, Wang and Yang combined deep learning with traditional iteration to devise the Int-Deep for solving low-dimensional PDEs with a finite element accuracy [30]. Dong and Li combined the ideas of domain decomposition and extreme learning to form a new deep learning method for PDEs [14].

Though deep learning-based methods have been proposed to handle variational inequalities in [30], to the best of our knowledge, there is no study on HVIs in the literature. In this paper, we propose a deep learning-based method to solve an elliptic HVI based on its equivalent variational form [22] and compare the numerical performance of three different training strategies for updating parameters. In our method, the solution space of the HVI is parameterized via DNNs and an approximation is found by minimizing an unconstrained expectation minimization problem, which can be solved by stochastic gradient descent methods or its variants (cf. [6]). In particular, the unconstrained expectation minimization problem is reformulated based on the variational principle of the HVI. Therefore, the resulting deep learning optimization problem has a clear physical meaning. In the meantime, we compare three algorithms for training networks: the classical stochastic algorithm with basic neural network parametrization, a blockwise training algorithm for multi-block neural networks, and an adaptive mesh-free multigrid algorithm. As applications, we employ the deep learning method to a frictional bilateral contact problem and a frictionless contact problem with normal compliance. As we shall see in the numerical experiments, the deep learning method is efficient in solving HVIs and the adaptive mesh-free multigrid algorithm can provide the most accurate solution among the three learning methods discussed. Finally, it deserves to emphasize that our method is easy to be implemented in programming and suitable for practical applications.

The rest of this paper is organized as follows. In Section 2, an elliptic HVI and its applications in contact mechanics are introduced briefly. In Section 3, the deep learning method as well as three training algorithms for solving the HVI are presented in details. In Section 4, two numerical

examples are provided to demonstrate the efficiency of the deep learning methods. Finally, we summarize our work with a short conclusion in Section 5.

2 The elliptic hemivariational inequality with applications

In this section, we first introduce some notations. For a real Banach space X equipped with a norm $\|\cdot\|_X$, denote by X^* its dual space equipped with a norm $\|\cdot\|_{X^*}$. The notation $\langle \cdot, \cdot \rangle$ stands for the dual pairing between X^* and X . These notations apply to a Hilbert space H naturally. Denote by $\mathcal{L}(X, Y)$ the space of all continuous linear operators from one normed linear space X to another normed linear space Y . We also use the standard notations for Sobolev spaces and norms or seminorms (cf. [1]). For any locally Lipschitz continuous functional j on a Banach space X , denote by $j^0(u; w)$ the generalized (Clarke) directional derivative of j at u in the direction w (cf. [10, 11]); i.e.,

$$j^0(u; w) = \limsup_{v \rightarrow u, t \downarrow 0} \frac{j(v + tw) - j(v)}{t}, \quad u \in X, w \in X.$$

2.1 The elliptic hemivariational inequality and its equivalent minimization problem

In this paper, we consider an elliptic HVI on a spatial domain Ω in a finite-dimensional Euclidean space. For simplicity, we denote the boundary or part of the boundary of the domain as Γ . Let H be a Hilbert space. The elliptic HVI can be described as follows.

Problem 1 Find $u \in H$ such that

$$\langle Au, v \rangle + \int_{\Gamma} j^0(\gamma_j u; \gamma_j v) ds \geq \langle f, v \rangle, \quad v \in H, \quad (2.1)$$

where $j : \Gamma \times \mathbb{R}^m \rightarrow \mathbb{R}$ is a locally Lipschitz continuous functional for some positive integer m , $\gamma_j \in \mathcal{L}(H, L^2(\Gamma; \mathbb{R}^m))$. In the study of Problem 1, we need the following assumptions [22]:

(A1) $A : H \rightarrow H^*$ is Lipschitz continuous and strongly monotone; i.e., for a constant $m_A > 0$,

$$\langle Av_1 - Av_2, v_1 - v_2 \rangle \geq m_A \|v_1 - v_2\|_H^2, \quad v_1, v_2 \in H.$$

(A2) $j(\cdot, \mathbf{z})$ is measurable on Γ , $\mathbf{z} \in \mathbb{R}^m$; there exists $\mathbf{z} \in L^2(\Gamma; \mathbb{R}^m)$ such that $j(\cdot, \mathbf{z}(\cdot)) \in L^1(\Gamma)$;

there exist non-negative constants c_0, c_1 , and α_j such that

$$\begin{aligned} \|\partial j(\mathbf{z})\|_{\mathbb{R}^m} &\leq c_0 + c_1 \|\mathbf{z}\|_{\mathbb{R}^m}, \quad \mathbf{z} \in \mathbb{R}^m, \\ j^0(\mathbf{z}_1; \mathbf{z}_2 - \mathbf{z}_1) + j^0(\mathbf{z}_2; \mathbf{z}_1 - \mathbf{z}_2) &\leq \alpha_j \|\mathbf{z}_1 - \mathbf{z}_2\|_{\mathbb{R}^m}^2, \quad \mathbf{z}_1, \mathbf{z}_2 \in \mathbb{R}^m. \end{aligned}$$

(A3) $f \in H^*$.

(A4) Denote by c_{Γ} an upper bound of the norm of the operator γ_j . There holds

$$\|\gamma_j v\|_{L^2(\Gamma; \mathbb{R}^m)} \leq c_{\Gamma} \|v\|_H, \quad v \in H.$$

We recall an important result on the solution existence and uniqueness for Problem 1 (cf. [25]).

Theorem 2.1. Assume (A1)-(A4) and $\alpha_j c_{\Gamma}^2 < m_A$ hold true. For any given $f \in H^*$, Problem 1 has a unique solution.

Next, assume $A \in \mathcal{L}(H, H^*)$ is symmetric, i.e.,

$$\langle Av_1, v_2 \rangle = \langle Av_2, v_1 \rangle, \quad v_1, v_2 \in H.$$

We turn to consider the following minimization problem:

Problem 2 Find $u \in H$ such that

$$u = \arg \min_{v \in H} E(v), \quad (2.2)$$

where

$$E(v) = \frac{1}{2} \langle Av, v \rangle + \int_{\Gamma} j(\gamma_j v) \, ds - \langle f, v \rangle, \quad v \in H.$$

As given in [22], we have the following equivalence result.

Theorem 2.2. *Assume (A1)-(A4), $\alpha_j c_{\Gamma}^2 < m_A$, and $A \in \mathcal{L}(H, H^*)$ is symmetric. Then Problem 2 is equivalent to Problem 1.*

Note that the functional $E(v)$ in (2.2) is reformulated from (2.1) based on the variational principle. Hence, it has clear physical meaning in mechanics.

2.2 Some applications in contact mechanics

Let $\Omega \subset \mathbb{R}^2$ be the reference configuration of a linear elastic body. We assume that Ω is an open, bounded, and connected domain with Lipschitz continuous boundary $\Gamma = \partial\Omega$. The boundary is made of three disjoint and measurable parts: Γ_D , Γ_T , and Γ_C such that $\text{meas}(\Gamma_D) > 0$ and $\text{meas}(\Gamma_C) > 0$. Denote by \cdot and $|\cdot|$ the canonical inner product and the induced norm, respectively. For a vector field $\mathbf{v} \in \mathbb{R}^2$, we use $v_{\nu} = \mathbf{v} \cdot \boldsymbol{\nu}$ for its normal component and $\mathbf{v}_{\tau} = \mathbf{v} - v_{\nu} \boldsymbol{\nu}$ for its tangential component, where $\boldsymbol{\nu}$ is the unit outward normal vector to Γ . The linearized strain tensor associated with a displacement field $\mathbf{u} : \Omega \rightarrow \mathbb{R}^2$ is denoted by $\boldsymbol{\varepsilon}(\mathbf{u})$ and the stress field is denoted by $\boldsymbol{\sigma} : \Omega \rightarrow \mathbb{S}^2$. In addition, we assume a volume force of density $\mathbf{f}_0 \in L^2(\Omega, \mathbb{R}^2)$ acting in Ω . Besides, the body is assumed to be fixed on Γ_D , is subject to an action of the surface traction of density $\mathbf{f}_2 \in L^2(\Gamma_T, \mathbb{R}^2)$ on Γ_T , and is in contact on Γ_C . We usually drop the spatial variable \mathbf{x} for simplicity when the dependence is clear without any confusion.

To discuss the contact problem, we introduce a space

$$V = \{\mathbf{v} \in H^1(\Omega; \mathbb{R}^2) | \mathbf{v} = \mathbf{0} \text{ a.e. on } \Gamma_D\}$$

equipped with the inner product

$$(\mathbf{u}, \mathbf{v})_V = \int_{\Omega} \boldsymbol{\varepsilon}(\mathbf{u}) \cdot \boldsymbol{\varepsilon}(\mathbf{v}) \, dx, \quad \mathbf{u}, \mathbf{v} \in V,$$

and the associated norm $\|\mathbf{v}\|_V = \sqrt{(\mathbf{v}, \mathbf{v})_V}$. Thanks to $\text{meas}(\Gamma_D) > 0$ and Korn's inequality [7], we know V is a Hilbert space with the norm $\|\cdot\|_V$. Besides, we need to introduce another Hilbert space $Q = L^2(\Omega; \mathbb{S}^2)$, which is equipped with the inner product

$$(\boldsymbol{\sigma}, \boldsymbol{\tau})_Q = \int_{\Omega} \sigma_{ij}(\mathbf{x}) \tau_{ij}(\mathbf{x}) \, dx.$$

Here and below, we use the Einstein summation convention, which means the summation is implied for an index exactly appeared two times in a quantity.

First of all, we introduce an HVI to describe the frictional bilateral contact problem (cf. [19, 25]). We let

$$V_1 = \{\mathbf{v} \in V | v_{\nu} = 0 \text{ on } \Gamma_C\},$$

and define

$$\begin{aligned}
\langle A\mathbf{u}, \mathbf{v} \rangle &= (\mathcal{F}(\boldsymbol{\varepsilon}(\mathbf{u})), \boldsymbol{\varepsilon}(\mathbf{v}))_Q; \\
\gamma_{j_\tau} : V_1 &\rightarrow L^2(\Gamma_C; \mathbb{R}^2) \text{ such that } \gamma_{j_\tau}(\mathbf{v}) = \mathbf{v}_\tau; \\
\int_{\Gamma} j^0(\gamma_j \mathbf{u}; \gamma_j \mathbf{v}) \, ds &= \int_{\Gamma_C} j_\tau^0(\gamma_{j_\tau} \mathbf{u}; \gamma_{j_\tau} \mathbf{v}) \, ds; \\
\langle \mathbf{f}, \mathbf{v} \rangle &= \int_{\Omega} \mathbf{f}_0 \cdot \mathbf{v} \, dx + \int_{\Gamma_T} \mathbf{f}_2 \cdot \mathbf{v} \, ds, \quad \mathbf{v} \in V;
\end{aligned}$$

where the linear elasticity operator $\mathcal{F} = (F_{ijkl})_{1 \leq i,j,k,l \leq 2} : \Omega \times \mathbb{S}^2 \rightarrow \mathbb{S}^2$ is symmetric, bounded, and satisfies the following property [22]

$$\mathcal{F}(\boldsymbol{\sigma}) \cdot \boldsymbol{\sigma} \geq m_{\mathcal{F}} |\boldsymbol{\sigma}|^2, \quad m_{\mathcal{F}} > 0, \quad \boldsymbol{\sigma} \in \mathbb{S}^2, \quad (2.3)$$

$j_\tau : \Gamma_C \times \mathbb{R}^2 \rightarrow \mathbb{R}$ is locally Lipschitz on \mathbb{R}^2 for a.e. $\mathbf{x} \in \Gamma_C$ and satisfies the assumption (A2) with constants c_0 , c_1 and α_{j_τ} (cf. [19, 25]). Then the frictional bilateral contact problem can be described as a HVI in the form

$$(\mathcal{F}(\boldsymbol{\varepsilon}(\mathbf{u})), \boldsymbol{\varepsilon}(\mathbf{v}))_Q + \int_{\Gamma_C} j_\tau^0(\mathbf{u}_\tau; \mathbf{v}_\tau) \, ds \geq \langle \mathbf{f}, \mathbf{v} \rangle, \quad \mathbf{v} \in V_1. \quad (2.4)$$

Let $\mathbf{u} \in V_1$ and λ_1 be the smallest positive eigenvalue of the eigenvalue problem

$$\int_{\Omega} \boldsymbol{\varepsilon}(\mathbf{u}) \cdot \boldsymbol{\varepsilon}(\mathbf{v}) \, dx = \lambda_1 \int_{\Gamma_C} \mathbf{u}_\tau \cdot \mathbf{v}_\tau \, ds, \quad \mathbf{v} \in V_1.$$

Then the assumption (A4) is satisfied if $c_\Gamma \geq \sqrt{1/\lambda_1}$ holds true.

The assumption (A1) is satisfied with $m_A = m_{\mathcal{F}}$. Following Theorem 2.1 and Theorem 2.2, if $\alpha_{j_\tau} < \lambda_1 m_{\mathcal{F}}$, (2.4) has a unique solution and is equivalent to the following optimization problem:

$$\mathbf{u} = \arg \min_{\mathbf{v} \in V_1} E(\mathbf{v}), \quad (2.5)$$

where

$$E(\mathbf{v}) = \frac{1}{2} (\mathcal{F}(\boldsymbol{\varepsilon}(\mathbf{v})), \boldsymbol{\varepsilon}(\mathbf{v}))_Q + \int_{\Gamma_C} j_\tau(\mathbf{v}_\tau) \, ds - \langle \mathbf{f}, \mathbf{v} \rangle.$$

Next, we introduce an HVI to describe the frictionless normal compliance contact problem (cf. [19, 25]). Define

$$\begin{aligned}
\langle A\mathbf{u}, \mathbf{v} \rangle &= (\mathcal{F}(\boldsymbol{\varepsilon}(\mathbf{u})), \boldsymbol{\varepsilon}(\mathbf{v}))_Q; \\
\gamma_{j_\nu} : V &\rightarrow L^2(\Gamma_C) \text{ such that } \gamma_{j_\nu}(\mathbf{v}) = \mathbf{v}_\nu; \\
\int_{\Gamma} j^0(\gamma_j \mathbf{u}; \gamma_j \mathbf{v}) \, ds &= \int_{\Gamma_C} j_\nu^0(\gamma_{j_\nu} \mathbf{u}; \gamma_{j_\nu} \mathbf{v}) \, ds; \\
\langle \mathbf{f}, \mathbf{v} \rangle &= \int_{\Omega} \mathbf{f}_0 \cdot \mathbf{v} \, dx + \int_{\Gamma_T} \mathbf{f}_2 \cdot \mathbf{v} \, ds, \quad \mathbf{v} \in V;
\end{aligned}$$

where the linear elasticity operator $\mathcal{F} = (F_{ijkl})_{1 \leq i,j,k,l \leq 2} : \Omega \times \mathbb{S}^2 \rightarrow \mathbb{S}^2$ is symmetric, bounded, and satisfies (2.3) (cf. [22]). $j_\nu : \Gamma_C \times \mathbb{R} \rightarrow \mathbb{R}$ is locally Lipschitz on \mathbb{R} for a.e. $\mathbf{x} \in \Gamma_C$ and satisfies the assumption (A2) with constants c_0 , c_1 and α_{j_ν} (cf. [19, 25]).

Therefore, the frictionless normal compliance contact problem reads

$$(\mathcal{F}(\varepsilon(\mathbf{u})), \varepsilon(\mathbf{v}))_Q + \int_{\Gamma_C} j_\nu^0(\mathbf{u}_\nu; \mathbf{v}_\nu) \, ds \geq \langle \mathbf{f}, \mathbf{v} \rangle, \quad \mathbf{v} \in V. \quad (2.6)$$

Let $\mathbf{u} \in V$ and λ_2 be the smallest positive eigenvalue of the eigenvalue problem

$$\int_{\Omega} \varepsilon(\mathbf{u}) \cdot \varepsilon(\mathbf{v}) \, dx = \lambda_2 \int_{\Gamma_C} \mathbf{u}_\nu \cdot \mathbf{v}_\nu \, ds, \quad \mathbf{v} \in V.$$

Then the assumption (A4) is satisfied if $c_\Gamma \geq \sqrt{1/\lambda_2}$ holds true. The assumption (A1) is satisfied with $m_A = m_{\mathcal{F}}$. Following Theorem 2.1 and Theorem 2.2, if $\alpha_{j_\nu} < \lambda_2 m_{\mathcal{F}}$, (2.6) has a unique solution and is equivalent to the following optimization problem:

$$\mathbf{u} = \arg \min_{\mathbf{v} \in V} E(\mathbf{v}), \quad (2.7)$$

where

$$E(\mathbf{v}) = \frac{1}{2}(\mathcal{F}(\varepsilon(\mathbf{v})), \varepsilon(\mathbf{v}))_Q + \int_{\Gamma_C} j_\nu(\mathbf{v}_\nu) \, ds - \langle \mathbf{f}, \mathbf{v} \rangle.$$

3 Deep learning-based methods for HVIs

3.1 The deep learning method

The main idea of deep learning-based HVIs solvers is to treat DNNs as an efficient parametrization of the solution space of an HVI. The HVI solution is identified via seeking a DNN $\phi(\mathbf{x}, \boldsymbol{\theta})$ with input \mathbf{x} and parameters $\boldsymbol{\theta}$ that minimizes the variational minimization problem related to the HVI. From the discussion in Section 2, we know that Problem 1 is equivalent to Problem 2. This motivates the following problem.

Problem 3 Find $\boldsymbol{\theta}^*$ such that

$$\boldsymbol{\theta}^* = \arg \min_{\boldsymbol{\theta}} E(\phi(\mathbf{x}; \boldsymbol{\theta})), \quad (3.1)$$

where

$$E(\phi(\mathbf{x}; \boldsymbol{\theta})) = \frac{1}{2} \langle A\phi(\mathbf{x}; \boldsymbol{\theta}), \phi(\mathbf{x}; \boldsymbol{\theta}) \rangle + \int_{\Gamma} j(\gamma_j \phi(\mathbf{x}; \boldsymbol{\theta})) \, ds - \langle \mathbf{f}, \phi(\mathbf{x}; \boldsymbol{\theta}) \rangle. \quad (3.2)$$

In contact mechanics, the first and the third terms on the right-hand side of (3.2) usually can be formulated as the integrals. Then the objective function in (3.2) can be viewed as a sum of expectations of several random variables, which can be solved by stochastic gradient descent methods or its variants (cf. [6]). We refer to Subsection 4.1 for details along this line.

In this paper, we use two neural networks to approximate the solution of the HVI introduced in Section 2. The first one is the residual neural network (ResNet) proposed in [27].

Mathematically, the ResNet can be formulated as follow [15]:

$$\mathbf{h}_0 = \mathbf{V}\mathbf{x}, \quad \mathbf{g}_\ell = \sigma(\mathbf{W}_\ell \mathbf{h}_{\ell-1} + \mathbf{b}_\ell), \quad \mathbf{h}_\ell = \mathbf{h}_{\ell-1} + \mathbf{U}_\ell \mathbf{g}_\ell, \quad \ell = 1, 2, \dots, L, \quad \phi(\mathbf{x}; \boldsymbol{\theta}) = \mathbf{a}^T \mathbf{h}_L,$$

where $\mathbf{V} \in \mathbb{R}^{N_0 \times d}$, $\mathbf{W}_\ell \in \mathbb{R}^{N_\ell \times N_0}$, $\mathbf{U}_\ell \in \mathbb{R}^{N_0 \times N_\ell}$, $\mathbf{b}_\ell \in \mathbb{R}^{N_\ell}$ for $\ell = 1, \dots, L$, $\mathbf{a} \in \mathbb{R}^{N_0 \times m}$. $\sigma(x)$ is a non-linear activation function. For the purpose of simplicity, we consider $N_0 = N_\ell = N$ and \mathbf{U}_ℓ is set as the identity matrix. Here, L is the depth of the ResNet, and N is the width of the

network, and $\boldsymbol{\theta} = \{\mathbf{V}, \mathbf{a}, \mathbf{W}_\ell, \mathbf{b}_\ell : 1 \leq \ell \leq L\}$ denotes the set of all parameters in ϕ , which uniquely determines the neural network.

The other one is a special neural network consisting of an input block and a few parallel blocks as visualized in Figure 1. Precisely speaking, the whole network is denoted by $B(\mathbf{x}, \boldsymbol{\theta})$. The input block is a ResNet with width N_{in} and depth L_{in} denoted by $B_{in}(\mathbf{x}, \boldsymbol{\theta}_{in})$. Following the input block are P parallel blocks as independent ResNets with width N_p and depth L_p denoted by $B_p(\mathbf{x}, \boldsymbol{\theta}_p)$ for $1 \leq p \leq P$. Then the network $B(\mathbf{x}, \boldsymbol{\theta})$ can be formulated as

$$B(\mathbf{x}, \boldsymbol{\theta}) = \sum_{p=1}^P B_p(B_{in}(\mathbf{x}, \boldsymbol{\theta}_{in}), \boldsymbol{\theta}_p)$$

In this network structure, different ResNets in parallel are trained with samples at different levels of discretization grids to obtain a PDE solution. The detailed training algorithm will be introduced later.

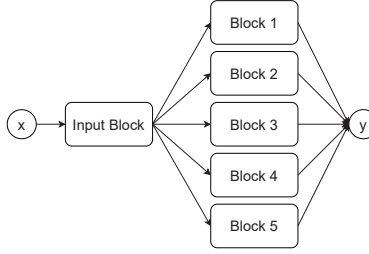


Figure 1: The illustration of the network $B(\mathbf{x}, \boldsymbol{\theta})$ with $P = 5$.

3.2 Three strategies for updating network parameters

Now let us introduce three different strategies to update the parameters of the networks. First of all, we introduce a basic training algorithm to obtain a numerical solution to the HVI in the form of a ResNet $\phi(\mathbf{x}; \boldsymbol{\theta})$ or the network $B(\mathbf{x}; \boldsymbol{\theta})$. This algorithm is summarized in Algorithm 1 below.

Algorithm 1 The basic training algorithm.

Require: The desired HVI.

Ensure: The parameter set $\boldsymbol{\theta}$ in the solution ResNet $\phi(\mathbf{x}; \boldsymbol{\theta})$ or the solution network $B(\mathbf{x}; \boldsymbol{\theta})$.

Set *Epoch* as the total iteration number, and assign N , N_Γ as the sample sizes in the domain Ω , the boundary Γ , respectively.

Initialize $\phi(\mathbf{x}; \boldsymbol{\theta})$ or $B(\mathbf{x}; \boldsymbol{\theta})$ following the default random initialization of PyTorch.

for $k = 1, \dots, \textit{Epoch}$ **do**

 Generate uniformly distributed samples $\{\mathbf{x}_i\}_{i=1}^N \subset \Omega$, $\{\mathbf{x}_i\}_{i=1}^{N_\Gamma} \subset \Gamma$.

 Update $\boldsymbol{\theta}$ using the gradient of (3.2) evaluated at the generated samples.

end for

Next, we introduce a blockwise training algorithm without utilizing multigrid sampling to obtain the approximate solution to the HVI in the form of the network $B(\mathbf{x}, \boldsymbol{\theta})$ introduced before. This algorithm can serve as a comparison to the adaptive multigrid training algorithm to be introduced later. It consists of two phases: the initialization phase and the refinement phase. In the initialization phase, we train the network $B(\mathbf{x}, \boldsymbol{\theta})$ by Algorithm 1 for \textit{Epoch}_{int} iterations. In the refinement phase, we train only one block $B_p(\mathbf{x}, \boldsymbol{\theta}_p)$ together with the input block (i.e., the

parameters in other blocks are fixed) in each iteration. We use $Epoch_{re}$ to denote the number of blockwise refinement steps and $Epoch_b$ to specify how many times a certain block is trained contiguously. Thus, the total training iterations in the refinement phase is $Epoch_{re} \times P \times Epoch_b$. The blockwise training algorithm is summarized in Algorithm 2 below.

Algorithm 2 The blockwise training algorithm.

Require: The desired HVI.

Ensure: The parameter set θ in the solution network $B(\mathbf{x}; \theta)$.

Set parameters $Epoch_{int}$, $Epoch_{re}$, and $Epoch_b$ as iteration numbers. Assign parameters N , N_Γ for sample sizes in the domain Ω , the boundary Γ , respectively. Let P be the number of blocks. Initialize $B(\mathbf{x}; \theta)$ following the default random initialization of PyTorch.

for $k = 1, \dots, Epoch_{int}$ **do**

 Generate uniformly distributed samples $\{\mathbf{x}_i\}_{i=1}^N \subset \Omega$, $\{\mathbf{x}_i\}_{i=1}^{N_\Gamma} \subset \Gamma$.

 Update θ using the gradient of (3.2) evaluated at the generated samples.

end for

for $j = 1, \dots, Epoch_{re}$ **do**

for $p = 1, \dots, P$ **do**

for $\ell = 1, \dots, Epoch_b$ **do**

 Generate uniformly distributed samples $\{\mathbf{x}_i\}_{i=1}^N \subset \Omega$, $\{\mathbf{x}_i\}_{i=1}^{N_\Gamma} \subset \Gamma$.

 Update all the parameters of the p -th block and the input block using the gradient of (3.2) evaluated at the sampled grid points just above.

end for

end for

end for

Since deep learning is challenging to obtain a very accurate solution to PDEs, we use some technical strategies for training the networks to improve the accuracy. It is well known that multi-grid methods improve solution accuracy via computation on a hierarchy of discretization meshes. Multigrid computation traverses from fine grids to coarse grids and finally back to fine grids so as to efficiently improve the solution error at different levels. The special order of traverse in multigrid methods is motivated by the fact that traditional iterative methods tend to reduce high-frequency errors better than low-frequency errors. In contrast, deep learning optimization reduces low-frequency errors faster than high-frequency errors as discussed in [60, 8]. Based on this observation, we propose a mesh-free multigrid method for training the parameters of the networks. A straightforward design of such a method would move the computation among different levels of grids in the opposite way of multigrid. However, the numerical performance is not satisfactory. To overcome this limitation, we adopt the adaptive strategy, that means, the computation moves from the current grids to the grids associated with the smallest loss function evaluated at the corresponding grids. This idea leads to an adaptive multigrid method described below.

Suppose there are P levels of grids generated by uniform discretization with step sizes $H, 2H, \dots, 2^{P-1}H$, where H is the step size of the finest grids. Let $Epoch_{int}$, $Epoch_{re}$, and $Epoch_b$ be the same parameters as in the blockwise training algorithm. This algorithm utilizing multigrid sampling also consists of an initialization phase and a refinement phase. The initialization phase of the adaptive multigrid training is the same as the one of the blockwise training algorithm. In the refinement phase, we first evaluate a loss E_p according to (3.2) using N samples from Ω_p^H , N_Γ samples from Γ_p^H , where Ω_p^H is the grids in the domain with a step size $2^{P-1}H$, Γ_p^H is the grids on the boundary Γ with a step size $2^{P-1}H$. If E_k is the smallest one among $\{E_p\}_{p=1}^P$, we then train the k -th block

and the input block with N samples from Ω_p^H , N_Γ samples from Γ_p^H . Thus, the total training iterations in the refinement phase is $Epoch_{re} \times Epoch_b$. Such a training algorithm chooses the grids corresponding to the smallest loss as training samples to refine the network parameters and, hence, it is called an adaptive multigrid training algorithm. See Algorithm 3 below for a detailed description.

Algorithm 3 The adaptive multigrid training.

Require: The desired HVI.

Ensure: The parameter set θ in the solution network $B(\mathbf{x}; \theta)$.

Set parameters $Epoch_{int}$, $Epoch_b$, and $Epoch_{re}$ as iteration numbers, parameters N and N_Γ as sample sizes in the domain Ω and the boundary Γ , respectively. Let P be the number of blocks.

Initialize $B(\mathbf{x}; \theta)$ following the default random initialization of PyTorch.

for $k = 1, \dots, Epoch_{int}$ **do**

 Generate uniformly distributed samples $\{\mathbf{x}_i\}_{i=1}^N \subset \Omega$, $\{\mathbf{x}_i\}_{i=1}^{N_\Gamma} \subset \Gamma$.

 Update θ using the gradient of (3.2) evaluated at the generated samples.

end for

for $j = 1, \dots, Epoch_{re}$ **do**

for $p = 1, \dots, P$ **do**

 Generate uniformly distributed samples $\{\mathbf{x}_i\}_{i=1}^N \subset \Omega_p^H$, $\{\mathbf{x}_i\}_{i=1}^{N_\Gamma} \subset \Gamma_p^H$.

 Evaluate the loss E_p according to (3.2) using the samples just above.

end for

 Let $p = \arg \min_{1 \leq p \leq P} E_p$.

for $\ell = 1, \dots, Epoch_b$ **do**

 Generate uniformly distributed samples $\{\mathbf{x}_i\}_{i=1}^N \subset \Omega_p^H$, $\{\mathbf{x}_i\}_{i=1}^{N_\Gamma} \subset \Gamma_p^H$.

 Update all the parameters of the p -th block and the input block using the gradient of (3.2) evaluated at the sampled grid points just above.

end for

end for

4 Numerical experiments

In this section, we shall illustrate the performance of the deep learning method to a frictional bilateral contact problem and a frictionless normal compliance contact problem. Numerical comparisons of the deep learning method and the virtual element method (VEM) are provided. As we will see, the approximation accuracy in the form of DNNs is nearly the same as that of VEM in a fine meshsize, but the deep learning method is much easier to implement. In the meantime, we investigate the numerical performance in terms of different network structures and different training algorithms. As we will see, the adaptive mesh-free multigrid algorithm can provide a more accurate approximation to HVIs than other deep learning methods.

4.1 The algorithm description of deep learning methods for contact problems

From Section 2, we know the frictional bilateral contact problem (2.4) is equivalent to optimization problem (2.5) and the frictionless normal compliance contact problem (2.6) is equivalent to (2.7). In order to numerically solve these problems by deep learning method, we need to parametrize the solution space of HVIs as introduced in Section 3 firstly. The solution spaces are V_1 for the frictional bilateral contact problem (2.5) and V for the frictionless normal compliance contact problem (2.7).

To deal with the constraints in the admissible spaces V_1 or V , a natural way is the penalty method that penalizes the loss function with extra terms to enforce these constraints. However, tuning parameters in the penalty method may be tedious in practice. Therefore, we construct DNNs satisfying these constraints automatically as follows:

$$\phi(\mathbf{x}; \boldsymbol{\theta}) = \mathbf{b}(\mathbf{x}) * \psi(\mathbf{x}; \boldsymbol{\theta}),$$

where $\mathbf{b}(\mathbf{x})$ is a known smooth vector-valued function such that $\phi = \mathbf{0}$ on the Dirichlet boundary Γ_D and $\phi_\nu = 0$ on the contact boundary Γ_C for the frictional bilateral contact problem, or $\phi = \mathbf{0}$ on the Dirichlet boundary Γ_D for the frictionless normal compliance contact problem; $\psi(\mathbf{x}; \boldsymbol{\theta})$ is an arbitrary DNN in $\{\psi(\mathbf{x}; \boldsymbol{\theta})\}_{\boldsymbol{\theta}} \approx H^1(\Omega; \mathbb{R}^2)$; and “ $*$ ” stands for the Hadamard product. Thus, (3.1) can be formulated as follows

$$\boldsymbol{\theta}^* = \arg \min_{\boldsymbol{\theta}} E(\mathbf{b}(\mathbf{x}) * \psi(\mathbf{x}; \boldsymbol{\theta})), \quad (4.1)$$

and $\mathbf{u}^{DL}(\mathbf{x}; \boldsymbol{\theta}^*) = \mathbf{b}(\mathbf{x}) * \psi(\mathbf{x}; \boldsymbol{\theta}^*)$ is the approximate solution to the target HVI.

Next, we discuss the specific form $E(\mathbf{b} * \psi)$ in (4.1) for the frictional bilateral contact problem (2.5) and the frictionless normal compliance contact problem (2.7), respectively.

For the frictional bilateral contact problem (2.5),

$$\begin{aligned} & E(\mathbf{b}(\mathbf{x}) * \psi(\mathbf{x}; \boldsymbol{\theta})) \\ &= \frac{1}{2}(\mathcal{F}(\varepsilon(\mathbf{b}(\mathbf{x}) * \psi(\mathbf{x}; \boldsymbol{\theta}))), \varepsilon(\mathbf{b}(\mathbf{x}) * \psi(\mathbf{x}; \boldsymbol{\theta}))_Q) + \int_{\Gamma_C} j_\tau((\mathbf{b} * \psi)_\tau(\mathbf{x}; \boldsymbol{\theta})) \, ds - \langle \mathbf{f}, \mathbf{b}(\mathbf{x}) * \psi(\mathbf{x}; \boldsymbol{\theta}) \rangle \\ &= |\Omega| \mathbb{E}_{\boldsymbol{\xi}_1} \left[\frac{1}{2} \mathcal{F}(\varepsilon(\mathbf{b}(\boldsymbol{\xi}_1) * \psi(\boldsymbol{\xi}_1; \boldsymbol{\theta})))_{ij} \varepsilon(\mathbf{b}(\boldsymbol{\xi}_1) * \psi(\boldsymbol{\xi}_1; \boldsymbol{\theta}))_{ij} - \mathbf{f}_0(\boldsymbol{\xi}_1) \cdot \mathbf{b}(\boldsymbol{\xi}_1) * \psi(\boldsymbol{\xi}_1; \boldsymbol{\theta}) \right] \\ &\quad - |\Gamma_T| \mathbb{E}_{\boldsymbol{\xi}_2} [\mathbf{f}_2(\boldsymbol{\xi}_2) \cdot \mathbf{b}(\boldsymbol{\xi}_2) * \psi(\boldsymbol{\xi}_2; \boldsymbol{\theta})] + |\Gamma_C| \mathbb{E}_{\boldsymbol{\xi}_3} [j_\tau((\mathbf{b} * \psi)_\tau(\boldsymbol{\xi}_3; \boldsymbol{\theta}))], \end{aligned} \quad (4.2)$$

with $\boldsymbol{\xi}_1$, $\boldsymbol{\xi}_2$, and $\boldsymbol{\xi}_3$ being random vectors following the uniform distribution over Ω , Γ_T , and Γ_C , respectively. In practice, the minimization problem (4.2) is solved by the stochastic gradient descent method [6] or its variants (e.g. Adam[35]) by randomly sampling the integral domains in the loss function. In each iteration of the optimization algorithm, a stochastic loss function defined below is minimized instead of the original loss function in (4.2):

$$\begin{aligned} & \hat{E}(\mathbf{b}(\mathbf{x}) * \psi(\mathbf{x}; \boldsymbol{\theta})) \\ &= \frac{|\Omega|}{N} \sum_{l=1}^N \left[\frac{1}{2} \mathcal{F}(\varepsilon(\mathbf{b}(\boldsymbol{\xi}_l) * \psi(\boldsymbol{\xi}_l; \boldsymbol{\theta})))_{ij} \varepsilon(\mathbf{b}(\boldsymbol{\xi}_l) * \psi(\boldsymbol{\xi}_l; \boldsymbol{\theta}))_{ij} - \mathbf{f}_0(\boldsymbol{\xi}_l) \cdot \mathbf{b}(\boldsymbol{\xi}_l) * \psi(\boldsymbol{\xi}_l; \boldsymbol{\theta}) \right] \\ &\quad - \frac{|\Gamma_T|}{N_T} \sum_{l=1}^{N_T} [\mathbf{f}_2(\boldsymbol{\eta}_l) \cdot \mathbf{b}(\boldsymbol{\eta}_l) * \psi(\boldsymbol{\eta}_l; \boldsymbol{\theta})] + \frac{|\Gamma_C|}{N_T} \sum_{l=1}^{N_C} [j_\tau((\mathbf{b} * \psi)_\tau(\boldsymbol{\zeta}_l; \boldsymbol{\theta}))], \end{aligned} \quad (4.3)$$

where $\{\boldsymbol{\xi}_i\}_{i=1}^N$, $\{\boldsymbol{\eta}_i\}_{i=1}^{N_T}$, and $\{\boldsymbol{\zeta}_i\}_{i=1}^{N_C}$ are independent random vectors following the uniform distribution over Ω , Γ_T , and Γ_C , respectively.

Similarly, for the frictionless normal compliance contact problem (2.7),

$$\begin{aligned}
& E(\mathbf{b}(\mathbf{x}) * \psi(\mathbf{x}; \boldsymbol{\theta})) \\
&= \frac{1}{2}(\mathcal{F}(\varepsilon(\mathbf{b}(\mathbf{x}) * \psi(\mathbf{x}; \boldsymbol{\theta}))), \varepsilon(\mathbf{b}(\mathbf{x}) * \psi(\mathbf{x}; \boldsymbol{\theta}))_Q + \int_{\Gamma_C} j_\nu((b * \psi)_\nu(\mathbf{x}; \boldsymbol{\theta})) \, ds - \langle \mathbf{f}, \mathbf{b}(\mathbf{x}) * \psi(\mathbf{x}; \boldsymbol{\theta}) \rangle \\
&= |\Omega| \mathbb{E}_{\boldsymbol{\xi}_1} \left[\frac{1}{2} \mathcal{F}(\varepsilon(\mathbf{b}(\boldsymbol{\xi}_1) * \psi(\boldsymbol{\xi}_1; \boldsymbol{\theta})))_{ij} \varepsilon(\mathbf{b}(\boldsymbol{\xi}_1) * \psi(\boldsymbol{\xi}_1; \boldsymbol{\theta}))_{ij} - \mathbf{f}_0(\boldsymbol{\xi}_1) \cdot \mathbf{b}(\boldsymbol{\xi}_1) * \psi(\boldsymbol{\xi}_1; \boldsymbol{\theta}) \right] \\
&\quad - |\Gamma_T| \mathbb{E}_{\boldsymbol{\xi}_2} [\mathbf{f}_2(\boldsymbol{\xi}_2) \cdot \mathbf{b}(\boldsymbol{\xi}_2) * \psi(\boldsymbol{\xi}_2; \boldsymbol{\theta})] + |\Gamma_C| \mathbb{E}_{\boldsymbol{\xi}_3} [j_\nu((b * \psi)_\nu(\boldsymbol{\xi}_3; \boldsymbol{\theta}))], \tag{4.4}
\end{aligned}$$

with $\boldsymbol{\xi}_1$, $\boldsymbol{\xi}_2$, and $\boldsymbol{\xi}_3$ being random vectors following the uniform distribution over Ω , Γ_T , and Γ_C , respectively. In the implementation of stochastic optimization algorithm, the loss function evaluated in each iteration is defined as

$$\begin{aligned}
& \hat{E}(\mathbf{b}(\mathbf{x}) * \psi(\mathbf{x}; \boldsymbol{\theta})) \\
&= \frac{|\Omega|}{N} \sum_{l=1}^N \left[\frac{1}{2} \mathcal{F}(\varepsilon(\mathbf{b}(\boldsymbol{\xi}_l) * \psi(\boldsymbol{\xi}_l; \boldsymbol{\theta})))_{ij} \varepsilon(\mathbf{b}(\boldsymbol{\xi}_l) * \psi(\boldsymbol{\xi}_l; \boldsymbol{\theta}))_{ij} - \mathbf{f}_0(\boldsymbol{\xi}_l) \cdot \mathbf{b}(\boldsymbol{\xi}_l) * \psi(\boldsymbol{\xi}_l; \boldsymbol{\theta}) \right] \\
&\quad - \frac{|\Gamma_T|}{N_T} \sum_{l=1}^{N_T} [\mathbf{f}_2(\boldsymbol{\eta}_l) \cdot \mathbf{b}(\boldsymbol{\eta}_l) * \psi(\boldsymbol{\eta}_l; \boldsymbol{\theta})] + \frac{|\Gamma_C|}{N_C} \sum_{l=1}^{N_C} [j_\nu((b * \psi)_\nu(\boldsymbol{\zeta}_l; \boldsymbol{\theta}))], \tag{4.5}
\end{aligned}$$

where $\{\boldsymbol{\xi}_i\}_{i=1}^N$, $\{\boldsymbol{\eta}_i\}_{i=1}^{N_T}$, and $\{\boldsymbol{\zeta}_i\}_{i=1}^{N_C}$ are independent random vectors following the uniform distribution over Ω , Γ_T , and Γ_C , respectively.

4.2 Numerical results

In our numerical experiments, we apply the ResNet $\phi(\mathbf{x}; \boldsymbol{\theta})$ or the special block ResNet $\mathbf{B}(\mathbf{x}; \boldsymbol{\theta})$ introduced in Section 3 as the solution ansatz to HVIs. In the ResNet, we set the depth of ϕ as $L = 8$ and the width as $N = 50$. In the block ResNet \mathbf{B} , we take a ResNet with depth $L = 4$ and width $N = 50$ as the input block and take a ResNet with depth $L = 4$ and width $N = 10$ as each part in the parallel block. Therefore, the total number of parameters in $\phi(\mathbf{x}; \boldsymbol{\theta})$ is about 20,400 and the total number of $\mathbf{B}(\mathbf{x}; \boldsymbol{\theta})$ is about 12,400. Note that if we choose $\sigma(x) = \text{ReLU}(x)$, the derivative of the corresponding DNN is a constant almost everywhere, which leads to DNNs not being able to capture the feature of the PDE solution. In the literature, the activation function ReLU^α or \tanh are used for different problem, where $\text{ReLU}(x) = \max\{x, 0\}$ and α is a positive integer, to overcome this difficulty. All neural networks are trained by Adam optimizer [35] with a default learning rate $\eta = 0.001$ and exponential decay rates $\beta_1 = 0.9$ and $\beta_2 = 0.999$. The batch size in the domain is 1024 and the number of training dates on each boundary is 256 for all problems. All numerical experiments are implemented in Python 3.7 using Pytorch 1.3 in an Nvidia GEFORCE RTX 2080 Ti GPU card.

Before reporting numerical results, let us summarize notations used in this section. Denote by $\mathbf{u}^{DL} = (u_1^{DL}, u_2^{DL})^T$ as the approximate solution estimated by the deep learning method. Suppose \mathcal{T}_h is a uniform triangulation of Ω into K and $h = \text{diam}(K)$. Since the true solution is unavailable, for the bilateral contact problem, we use \mathbf{u}^{ref} as the reference solution evaluated by VEM with $h = 2^{-7}$ (see [19]). Similarly, for the frictionless contact with normal compliance problem, we take \mathbf{u}^{ref} as the reference solution evaluated by VEM with $h = 2^{-9}$ (see [19]). Denote the relative difference between the deep learning solution and the reference solution as

$$\mathcal{E}_r = \frac{\|\mathbf{u}^{DL} - \mathbf{u}^{ref}\|_E}{\|\mathbf{u}^{ref}\|_E},$$

where the energy norm $\|\cdot\|_E$ is defined by

$$\|\mathbf{v}\|_E = \frac{1}{\sqrt{2}} (\mathcal{F}(\boldsymbol{\varepsilon}(\mathbf{v})), \boldsymbol{\varepsilon}(\mathbf{v}))_Q^{1/2}.$$

Example 4.1. Consider the bilateral contact problem (2.4). The domain $\Omega = (0, 4) \times (0, 4)$ is the cross section of a three-dimensional linearly elastic body and the plane stress condition is imposed. The body is clamped on $\Gamma_D = \{4\} \times (0, 4)$ and vertical tractions act on $\Gamma_T = (\{0\} \times (0, 4)) \cup ((0, 4) \times \{4\})$. The frictional contact happens on the boundary $\Gamma_C = (0, 4) \times \{0\}$. The linear elasticity tensor \mathcal{F} is

$$\mathcal{F}_{ij} = \frac{E\kappa}{(1-\kappa^2)}(\varepsilon_{11} + \varepsilon_{22})\delta_{ij} + \frac{E}{1+\kappa}\varepsilon_{ij}, \quad 1 \leq i, j \leq 2,$$

where E is the Young modulus, κ is the Poisson ratio of the material, and δ_{ij} is the Kronecker symbol. In numerical simulations, we use the following data

$$\begin{aligned} E &= 2000 \text{ daN/mm}^2, \quad \kappa = 0.4, \\ \mathbf{f}_0(x, y) &= (0, 0)^T \text{ daN/mm}^2 \text{ in } \Omega, \\ \mathbf{f}_2(x, y) &= \begin{cases} (200(5-y), -200)^T \text{ daN/mm}^2 & \text{on } \{0\} \times (0, 4) \\ (0, 0)^T \text{ daN/mm}^2 & \text{on } (0, 4) \times \{4\}, \end{cases} \\ j_\tau(\mathbf{z}) &= \int_0^{\|\mathbf{z}\|} 450e^{-2000t} + 450 \, dt, \quad \mathbf{z} = (x, y). \end{aligned}$$

Since that ReLU ^{α} activation function is still not appropriate in this problem because of the numerical overflow in the training process. We choose the tanh activation function in this example. Figure 2 shows the numerical solution in the form of ResNet after 50,000 epochs. The first row of Figure 2 displays each component of \mathbf{u}^{DL} in the domain whereas the second row shows the approximation on the contact boundary.

For the purpose of quantifying the accuracy of deep learning methods and comparing the efficiency of different networks and algorithms, we evaluate the relative error between the numerical solution and a reference solution obtained by VEM. For Algorithm 1, we train the network with 50,000 epochs either using the ResNet ϕ or the block ResNet \mathbf{B} . For Algorithm 2, we set $Epoch_{int} = 9000$, $Epoch_b = 1000$, and $Epoch_{re} = 9$. In order to make fair comparisons, we stop Algorithm 2 after 50,000 total epochs to update network parameters. For Algorithm 3, we set the discretization step size $H = 1/50$ and use $Epoch_{int} = 9000$, $Epoch_{re} = 41$, and $Epoch_b = 1000$.

From Table 1, we see that the relative errors are reduced to 5% nearly by all training algorithms. Besides, the number of parameters of ResNet ϕ is almost twice of the one of block ResNet \mathbf{B} , but the solution in the form of block ResNet \mathbf{B} is more accurate than the one of ResNet ϕ . Moreover, the adaptive mesh-free multigrid algorithm can provide a more accurate solution than others after the same number of epochs: 41.4% higher accuracy than the basic algorithm and 35.5% higher accuracy than the blockwise algorithm.

Table 1: The relative error of different algorithms for the bilateral contact problem. Algorithm 1: the basic algorithm in the literature. Algorithm 2: blockwise training. Algorithm 3: adaptive mesh-free multigrid training.

Algorithm	Algorithm 1 (ResNet ϕ)	Algorithm 1 (Block ResNet \mathbf{B})	Algorithm 2	Algorithm 3
\mathcal{E}_r	0.0481	0.0412	0.0437	0.0282

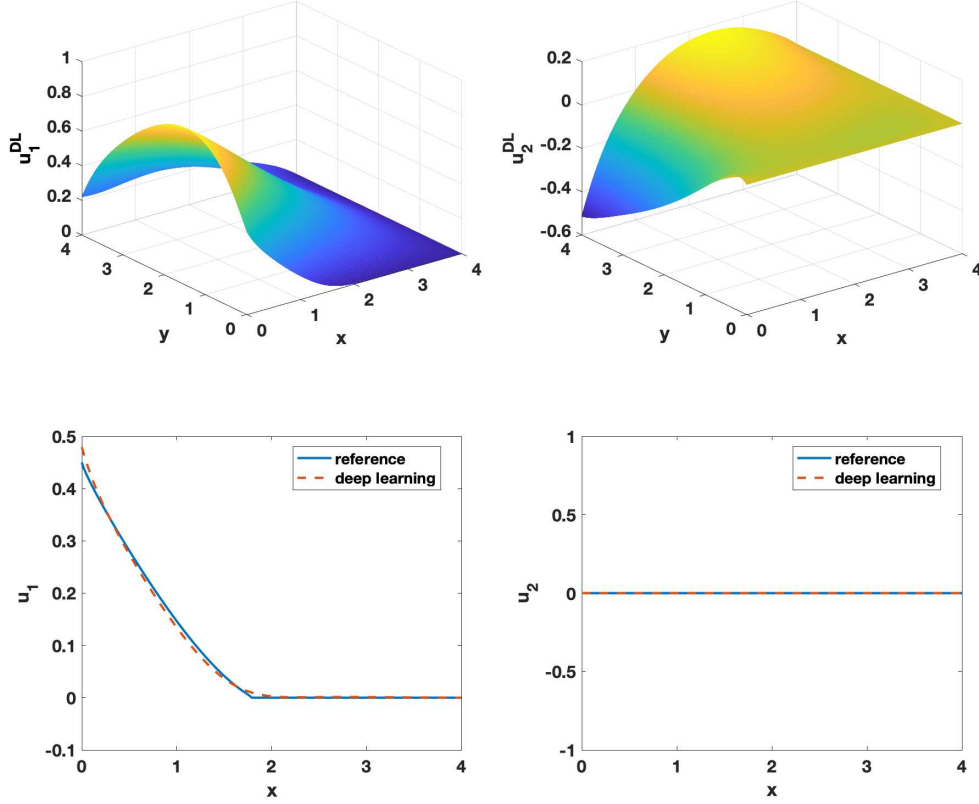


Figure 2: The numerical solution in the domain (upper) and on the contact boundary (bottom) of the bilateral contact problem.

Example 4.2. Consider the frictionless normal compliance contact problem (2.6). The domain $\Omega = (0, 1) \times (0, 1)$ is the cross section of a three-dimensional linearly elastic body and the plane stress condition is imposed. The body is clamped on $\Gamma_D = (\{0\} \times (0, 1)) \cup (\{1\} \times (0, 1))$ and the vertical traction acts on $\Gamma_T = (0, 1) \times \{1\}$. The frictional contact happens on the boundary $\Gamma_C = (0, 1) \times \{0\}$. The linear elasticity tensor \mathcal{F} is

$$\mathcal{F}_{ij} = \frac{E\kappa}{(1+\kappa)(1-2\kappa)}(\varepsilon_{11} + \varepsilon_{22})\delta_{ij} + \frac{E}{1+\kappa}\varepsilon_{ij}, \quad 1 \leq i, j \leq 2,$$

where E is the Young modulus, κ is the Poisson ratio of the material, and δ_{ij} is the Kronecker

symbol. In numerical simulations, we use the following data

$$\begin{aligned}
E &= 70 \text{ GPa}, \quad \kappa = 0.3, \\
\mathbf{f}_0(x, y) &= (0, 0)^T \text{ GPa} \quad \text{in } \Omega \\
\mathbf{f}_2(x, y) &= (0, -52)^T \text{ GPa} \quad \text{on } \Gamma_T \\
j_\nu(u_\nu) &= \begin{cases} 0, & u_\nu \leq 0, \\ 50u_\nu^2 + 0.1u_\nu, & u_\nu \in (0, 0.1], \\ 20.1u_\nu - 50u_\nu^2 - 1, & u_\nu \in (0.1, 0.15), \\ 200u_\nu^2 - 54.9u_\nu + 4.625, & u_\nu \geq 0.15. \end{cases}
\end{aligned}$$

The activation function $\text{ReLU}^2 = \max\{x^2, 0\}$ is chosen in this example based on numerical experience in this example. Figure 3 shows the numerical solution in the form of ResNet with activation function $\sigma(x) = \text{ReLU}^2$ after 50,000 epochs. The first row of Figure 3 displays each component of \mathbf{u}^{DL} in the domain whereas the second row shows the numerical solution on the contact boundary.

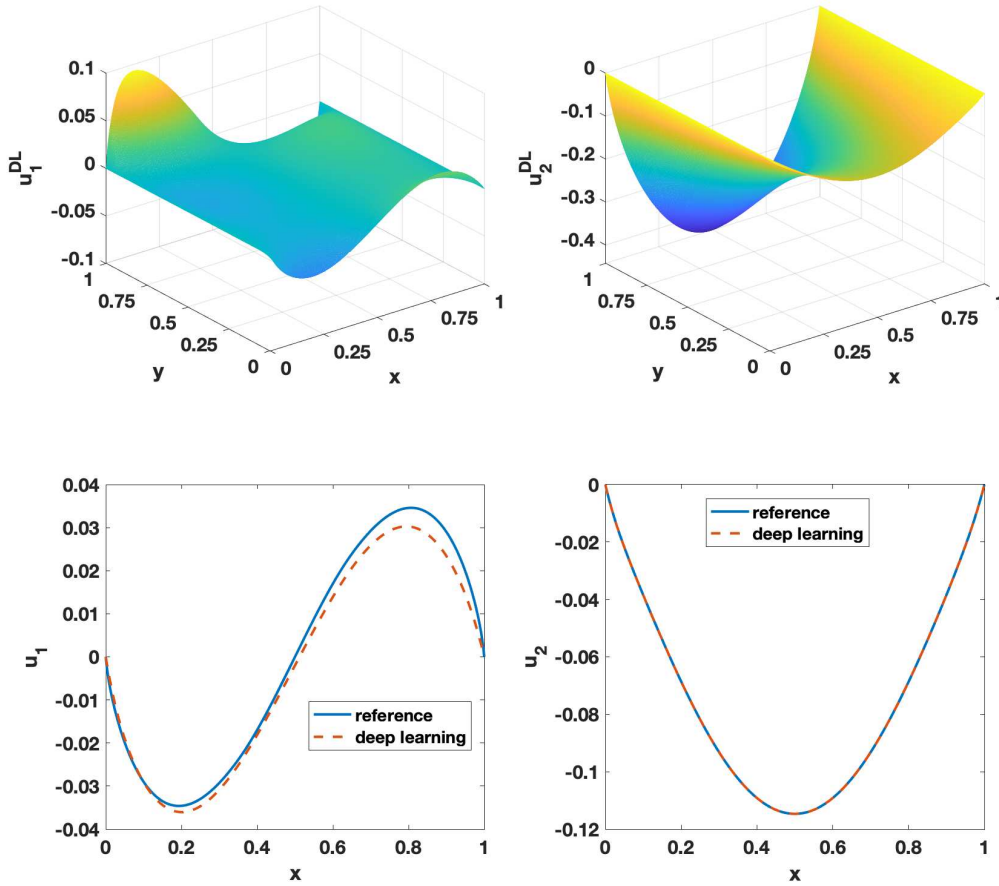


Figure 3: The numerical solution in the domain (upper) and on the contact boundary (bottom) of the frictionless normal compliance contact problem.

Similarly, we evaluate the relative error between the numerical solution and the reference solution to compare the numerical performance of different networks and different training algorithms. For Algorithm 1, we train the network with 50,000 epochs either using the ResNet ϕ or the block ResNet \mathbf{B} . For Algorithm 2, we set $Epoch_{int} = 9000$, $Epoch_b = 1000$, and $Epoch_{re} = 9$. In order to make a fair comparison, we stop Algorithm 2 after 50,000 total epochs. For Algorithm 3, we set the discretization step size $H = 1/200$ and use $Epoch_{int} = 9000$, $Epoch_{re} = 41$, and $Epoch_b = 1000$.

From Table 2, we see that relative errors are reduced to 7% by all deep learning methods. However, only the adaptive mesh-free multigrid algorithm can provide an approximate solution with a relative error less than 5% after 50,000 epochs. In particular, the adaptive mesh-free multigrid algorithm improves the accuracy by 38.4% compared to the basic algorithm and by 22.0% compared to the blockwise algorithm. At last, recall that the number of parameters of the ResNet ϕ is twice the one of the block ResNet \mathbf{B} , but the approximate solution in the form of the block ResNet \mathbf{B} is more accurate than the one of the ResNet ϕ .

Table 2: The relative error of different algorithms for the frictionless normal compliance contact problem. Algorithm 1: the basic algorithm in the literature. Algorithm 2: blockwise training. Algorithm 3: adaptive mesh-free multigrid training.

Algorithm	Algorithm 1 (ResNet ϕ)	Algorithm 1 (Block ResNet \mathbf{B})	Algorithm 2	Algorithm 3
\mathcal{E}_r	0.0706	0.0556	0.0558	0.0435

5 Conclusion

This paper focuses on developing a deep learning method for solving HVIs based on their variational problems. First of all, the solution space is parameterized via DNNs, and then the HVI is reformulated as an expectation minimization problem, which are therefore worked out by stochastic gradient descent method or its variants (e.g. Adam) combined with three different training strategies for updating network parameters. As applications to contact mechanics, a frictional bilateral contact problem and a frictionless normal compliance contact problem are carried out in details. Numerical results show that the deep learning method is efficient in solving HVIs and the adaptive mesh-free multigrid algorithm can provide the best accuracy solution among the three learning methods discussed. It deserves to mention that the proposed method is easy to realize in programming.

Acknowledgments

J. H. was partially supported by the National Key Research and Development Project (2020YFA0709800) and NSFC (Grant No. 12071289). C. W. was partially supported by National Science Foundation Award DMS-1849483. We would like to thank Dr. Fang Feng for offering the comparison data of numerical solutions for contact problems by the virtual element method used in numerical experiments.

References

- [1] R.A. Adams. *Sobolev Spaces*. Academic Press, New York-London, 1975.
- [2] C.C. Baniotopoulos, J. Haslinger, Z. Morávková. Mathematical modeling of delamination and nonmonotone friction problems by hemivariational inequalities. *Appl. Math.*, 50:1–25, 2005.

- [3] M. Barboteu, K. Bartosz, P. Kalita. An analytical and numerical approach to a bilateral contact problem with nonmonotone friction. *Int. J. Appl. Math. Comput. Sci.*, 23:263–276, 2013.
- [4] M. Barboteu, K. Bartosz, P. Kalita, A. Ramadan. Analysis of a contact problem with normal compliance, finite penetration and nonmonotone slip dependent friction. *Commun. Contemp. Math.*, 16:1350016, 29, 2014.
- [5] A. R. Barron. Universal approximation bounds for superpositions of a sigmoidal function. *IEEE Transactions on Information Theory*, 39:930–945, 1993.
- [6] L. Bottou, F. E. Curtis, J. Nocedal. Optimization methods for large-scale machine learning. *SIAM Rev.*, 60:223–311, 2018.
- [7] S. C. Brenner. Korn’s inequalities for piecewise H^1 vector fields. *Math. Comp.*, 73:1067–1087, 2004.
- [8] Y. Cao, Z. Fang, Y. Wu, D.-X. Zhou, Q. Gu. Towards Understanding the Spectral Bias of Deep Learning. *arXiv e-prints*, page arXiv:1912.01198, 2019.
- [9] F. Chen, J. Huang, C. Wang, H. Yang. Friedrichs Learning: Weak Solutions of Partial Differential Equations via Deep Learning. *arXiv e-prints*, page arXiv:2012.08023, 2020.
- [10] F.H. Clarke. Generalized gradients and applications. *Trans. Amer. Math. Soc.*, 205:247–262, 1975.
- [11] F.H. Clarke. *Optimization and nonsmooth analysis*. John Wiley & Sons, Inc., New York, 1983.
- [12] G. Cybenko. Approximation by superpositions of a sigmoidal function. *Math. Control Signals Systems*, 2:303–314, 1989.
- [13] M. W. M. G. Dissanayake, N. Phan-Thien. Neural-network-based approximations for solving partial differential equations. *Comm. Numer. Methods Engrg.*, 10:195–201, 1994.
- [14] S. Dong, Z. Li. Local extreme learning machines and domain decomposition for solving linear and nonlinear partial differential equations. *arXiv e-prints*, page arXiv:2012.02895, 2020.
- [15] W. E, C. Ma, Q. Wang. A Priori Estimates of the Population Risk for Residual Networks. *arXiv e-prints*, page arXiv:1903.02154, 2019.
- [16] W. E, C. Ma, L. Wu. A Priori Estimates of the Population Risk for Two-layer Neural Networks. *arXiv e-prints*, page arXiv:1810.06397, 2018.
- [17] W. E, S. Wojtowytsch. Representation formulas and pointwise properties for barron functions. *arXiv e-prints*, page arXiv:2006.05982, 2020.
- [18] W. E, B. Yu. The deep ritz method: a deep learning-based numerical algorithm for solving variational problems. *Commun. Math. Stat.*, 6:1–12, 2018.
- [19] F. Feng, W. Han, J. Huang. Virtual element method for an elliptic hemivariational inequality with applications to contact mechanics. *J. Sci. Comput.*, 81:2388–2412, 2019.
- [20] Y. Gu, H. Yang, C. Zhou. Selectnet: Self-paced learning for high-dimensional partial differential equations. *arXiv e-prints*, page arXiv:2001.04860, 2020.
- [21] J. Han, A. Jentzen, W. E. Solving high-dimensional partial differential equations using deep learning. *Proc. Natl. Acad. Sci. USA*, 115:8505–8510, 2018.
- [22] W. Han. Minimization principles for elliptic hemivariational inequalities. *Nonlinear Anal. Real World Appl.*, 54:103114, 13, 2020.
- [23] W. Han, S. Migórski, M. Sofonea. A class of variational-hemivariational inequalities with applications to frictional contact problems. *SIAM J. Math. Anal.*, 46:3891–3912, 2014.
- [24] W. Han, M. Sofonea. Numerical analysis of hemivariational inequalities in contact mechanics. *Acta Numer.*, 28:175–286, 2019.
- [25] W. Han, M. Sofonea, M. Barboteu. Numerical analysis of elliptic hemivariational inequalities. *SIAM J. Numer. Anal.*, 55:640–663, 2017.
- [26] J. Haslinger, M. Miettinen, P. D. Panagiotopoulos. *Finite element method for hemivariational inequalities*. Kluwer Academic Publishers, Dordrecht, 1999.
- [27] K. He, X. Zhang, S. Ren, J. Sun. Deep residual learning for image recognition. In *2016 IEEE Conference on Computer Vision and Pattern Recognition (CVPR)*, pages 770–778, 2016.
- [28] K. Hornik. Approximation capabilities of multilayer feedforward networks. *Neural Networks*, 4:251 – 257, 1991.
- [29] K. Hornik, M. Stinchcombe, H. White. Multilayer feedforward networks are universal approximators. *Neural Networks*, 2:359 – 366, 1989.

- [30] J. Huang, H. Wang, H. Yang. Int-deep: A deep learning initialized iterative method for nonlinear problems. *J. Comput. Phys.*, 419:109675, 24, 2020.
- [31] A. D. Jagtap, G. E. Karniadakis. Extended physics-informed neural networks (xpinns): A generalized space-time domain decomposition based deep learning framework for nonlinear partial differential equations. *Commun. Comput. Phys.*, 28:2002–2041, 2020.
- [32] A. D. Jagtap, K. Kawaguchi, G. E. Karniadakis. Adaptive activation functions accelerate convergence in deep and physics-informed neural networks. *J. Comput. Phys.*, 404:109136, 23, 2020.
- [33] K. Joki, A.M. Bagirov, N. Karmitsa, M.M. Mäkelä, S. Taheri. Double bundle method for finding Clarke stationary points in nonsmooth DC programming. *SIAM J. Optim.*, 28:1892–1919, 2018.
- [34] Y. Khoo, J. Lu, L. Ying. Solving for high-dimensional committor functions using artificial neural networks. *Res. Math. Sci.*, 6:1–13, 2019.
- [35] D. P. Kingma, J. Ba. Adam: a Method for Stochastic Optimization. *arXiv e-prints*, page arXiv:1412.6980, 2014.
- [36] V.A. Kovtunencko. A hemivariational inequality in crack problems. *Optimization*, 60:1071–1089, 2011.
- [37] V. Kůrková. Kolmogorov’s theorem and multilayer neural networks. *Neural Networks*, 5:501–506, 1992.
- [38] I.E. Lagaris, A. Likas, D. I. Fotiadis. Artificial neural networks for solving ordinary and partial differential equations. *IEEE Trans. Neural Networks*, 9:987–1000, 1998.
- [39] H. Lee, I. S. Kang. Neural algorithm for solving differential equations. *J. Comput. Phys.*, 91:110–131, 1990.
- [40] S. Liang, L. Lyu, C. Wang, H. Yang. Reproducing activation function for deep learning. *arXiv e-prints*, page arXiv:2101.04844, 2021.
- [41] J. Lu, Z. Shen, H. Yang, S. Zhang. Deep Network Approximation for Smooth Functions. *arXiv e-prints*, page arXiv:2001.03040, 2020.
- [42] M.M. Mäkelä. Survey of bundle methods for nonsmooth optimization. *Optim. Methods Softw.*, 17:1–29, 2002.
- [43] K.S. McFall, J. R. Mahan. Artificial neural network method for solution of boundary value problems with exact satisfaction of arbitrary boundary conditions. *IEEE Trans. Neural Networks*, 20:1221–1233, 2009.
- [44] S. Migórski, A. Ochal, M. Sofonea. *Nonlinear inclusions and hemivariational inequalities*. Springer, New York, 2013.
- [45] E.S. Mistakidis and P.D. Panagiotopoulos. Numerical treatment of problems involving nonmonotone boundary or stress-strain laws. *Computers & Structures*, 64:553 – 565, 1997.
- [46] H. Montanelli, Q. Du. New error bounds for deep relu networks using sparse grids. *SIAM J. Math. Data Sci.*, 1:78–92, 2019.
- [47] H. Montanelli, H. Yang. Error bounds for deep Relu networks using the Kolmogorov-Arnold superposition theorem. *arXiv e-prints*, page arXiv:1906.11945, 2019.
- [48] D. Motreanu, P. D. Panagiotopoulos. *Minimax theorems and qualitative properties of the solutions of hemivariational inequalities*. Kluwer Academic Publishers, Dordrecht, 1999.
- [49] Z. Naniewicz, P. D. Panagiotopoulos. *Mathematical theory of hemivariational inequalities and applications*. Marcel Dekker, Inc., New York, 1995.
- [50] P. D. Panagiotopoulos. Nonconvex energy functions. hemivariational inequalities and substationarity principles. *Acta Mech.*, 48:111–130, 1983.
- [51] P. D. Panagiotopoulos. *Hemivariational inequalities. Applications in Mechanics and Engineering*. Springer, Berlin, 1993.
- [52] M. Raissi, P. Perdikaris, G.E. Karniadakis. Physics-informed neural networks: a deep learning framework for solving forward and inverse problems involving nonlinear partial differential equations. *J. Comput. Phys.*, 378:686 – 707, 2019.
- [53] K. Rudd, S. Ferrari. A constrained integration (CINT) approach to solving partial differential equations using artificial neural networks. *Neurocomputing*, 155:277 – 285, 2015.
- [54] R. Shekari Beidokhti, A. Malek. Solving initial-boundary value problems for systems of partial differential equations using neural networks and optimization techniques. *J. Franklin Inst.*, 346:898 – 913, 2009.
- [55] Z. Shen, H. Yang, S. Zhang. Deep Network Approximation Characterized by Number of Neurons. *arXiv e-prints*, page arXiv:1906.05497, 2019.

- [56] J.W. Siegel, J. Xu. Approximation rates for neural networks with general activation functions. *Neural Networks*, 128:313 – 321, 2020.
- [57] J. Sirignano, K. Spiliopoulos. DGM: a deep learning algorithm for solving partial differential equations. *J. Comput. Phys.*, 375:1339 – 1364, 2018.
- [58] M.A. Tzaferopoulos, E.S. Mistakidis, C.D. Bisbos, P.D. Panagiotopoulos. Comparison of two methods for the solution of a class of nonconvex energy problems using convex minimization algorithms. *Comput. & Structures*, 57:959–971, 1995.
- [59] F. Wang, H. Qi. A discontinuous Galerkin method for an elliptic hemivariational inequality for semipermeable media. *Appl. Math. Lett.*, 109:106572, 8, 2020.
- [60] Z.-Q.J. Xu, Y. Zhang, T. Luo, Y. Xiao, Z. Ma. Frequency principle: Fourier analysis sheds light on deep neural networks. *Commun. Comput. Phys.*, 28:1746–1767, 2020.
- [61] D. Yarotsky. Error bounds for approximations with deep relu networks. *Neural Networks*, 94:103–114, 2017.
- [62] D. Yarotsky. Optimal approximation of continuous functions by very deep relu networks. In *31st Annual Conference on Learning Theory*, volume 75, pages 1–11. 2018.
- [63] Y. Zang, G. Bao, X. Ye, H. Zhou. Weak adversarial networks for high-dimensional partial differential equations. *J. Comput. Phys.*, 411:109409, 14, 2020.